





Article

First-Principles study of the electronic structure of LLM-105 crystal and (101) plane under high pressure

Gang He ¹, Wenkun Zhu ^{2,3,†,‡}, Zhiqiang Qiao ⁴, Zhengguo Chen ^{5*}, Jun Wen ⁶

¹ School of Computer Science and Technology, Southwest University of Science and Technology, Mianyang, 621010, PR China; ganghe@swust.edu.cn

² State Key Laboratory of Environment-friendly Energy Materials, School of Life Science and Engineering, Southwest University of Science and Technology, Mianyang, 621010, PR China; zhuwenkun@swust.edu.cn

³ National Co-innovation Center for Nuclear Waste Disposal and Environmental Safety, Southwest University of Science and Technology, Mianyang, 621010, PR China; zhuwenkun@swust.edu.cn

⁴ Institute of Chemical Materials, China Academy of Engineering Physics, Mianyang, 621000, PR China; qiaozq@caep.cn

⁵ NHC Key Laboratory of Nuclear Technology Medical Transformation, Mianyang Central Hospital, Mianyang, 621000, PR China; maiwang342@163.com

⁶ Institute of Civil Engineering and Architecture, Southwest University of Science and Technology, Mianyang, 621010, PR China; bme_junwen@swust.edu.cn

* Correspondence: maiwang342@163.com; Tel.: +86-0816-6390761

† Current address: Sichuan Civil-military Integration Institute, Southwest University of Science and Technology, Mianyang, 621010, PR China.

‡ These authors contributed equally to this work.

Abstract: The electronic structural evolution of LLM-105 crystal and the (101) plane of LLM-105 crystal under different pressures is investigated by the density functional theory (DFT) calculations and the surface properties of seven low-Miller-index planes of LLM-105 crystal were investigated in this study. The result demonstrates that the surface energy of (101) plane of LLM-105 is much smaller when compared with other low-Miller-index planes of LLM-105. In order to further investigate the stability of crystal structure and (101) plane of LLM-105 under different pressures, a series of pressures ranged from 0 GPa to 55 GPa were applied during the DFT calculation, and the result shows that the electronic structures of LLM-105 crystal and the (101) plane changed with the increase of external pressure and the evolution process of (101) plane is different from that of LLM-105 crystal structure.

Keywords: low-Miller-index; High pressure; (101) plane, DFT calculation

1. Introduction

2,6-diamino-3,5-dinitropyrazine-1-oxide ($C_4H_4N_6O_5$, LLM-105), as a new generation of energetic material and a typical nitro energetic materials, it was firstly synthesized by Lawrence Livermore National Laboratory in 1995. Comparing to commonly known energetic materials such as octahydro-1,3,5,7-tetranitro-1,3,5,7-tetrazocine (HMX) or 1, 3, 5-triamino-2, 4, 6-trinitrobenzene (TATB), LLM-105 presents a good safety performance and high energy density. For example, the drop-height value (Dh50) of LLM-105 is 117 cm and that of HMX is 30 cm. In the meantime, LLM-105 has high energy level which is equivalent to 85% of HMX and LLM-105 has 15% higher energy than that of TATB [1,2]. Due to these outstanding properties, LLM-105 presents good prospects for usage in boosters [3] or insensitive munitions (IM) [4].

As we can see in the crystal model of LLM-105 (presented in Figure 1), there are four formula units per unit cell of LLM-105 and the symmetry of LLM-105 is monoclinic with $P2_1/n$ space group. LLM-105 has an extensive network of $\pi - \pi$ stacking and hydrogen-bonds in its crystal structure as shown in Figure 1.

Many experimental and theoretical studies have been reported about the structural properties[5–7], synthesis[8] or electronic properties[2,9] of LLM-105. Gilardi and Butcher[5] reported that because of the inter-molecular hydrogen-bonding interactions, the LLM-105 consists of ruffled parallel sheets(LLM-105 unit) along the [101] direction, which may suggest that (101) plane of LLM-105 crystal is more stable than other planes of LLM-105. However, the electronic structure properties of different crystal planes of LLM-105 and the electronic structure evolution of the most stable plane of LLM-105 under different high pressure is rarely reported.

Figure 1 illustrates the Monoclinic $P2_1/n$ unit cell and its six principal faces. The unit cell is shown in the top left, with axes a , b , and c , and angles α , β , and γ . The faces are labeled as follows:

- (010): Yellow face
- (001): Green face
- (011): Pink face
- (110): Cyan face
- (101): Purple face
- (100): Red face
- (111): Blue face

Figure 2. Diagram of seven low-Miller-index planes.

2. Materials and Methods

The initial molecular structure of LLM-105 (Cambridge Structural Database: refcode YEKQAG03) [10] was obtained from the work by Liu et al.[9]. The models of seven low-Miller-index planes of LLM-105 were constructed by Visualizer module of Materials Studio software (MS2017). The models of seven low-Miller-index planes of LLM-105 are presented in Figure 3 under the same coordinate system.

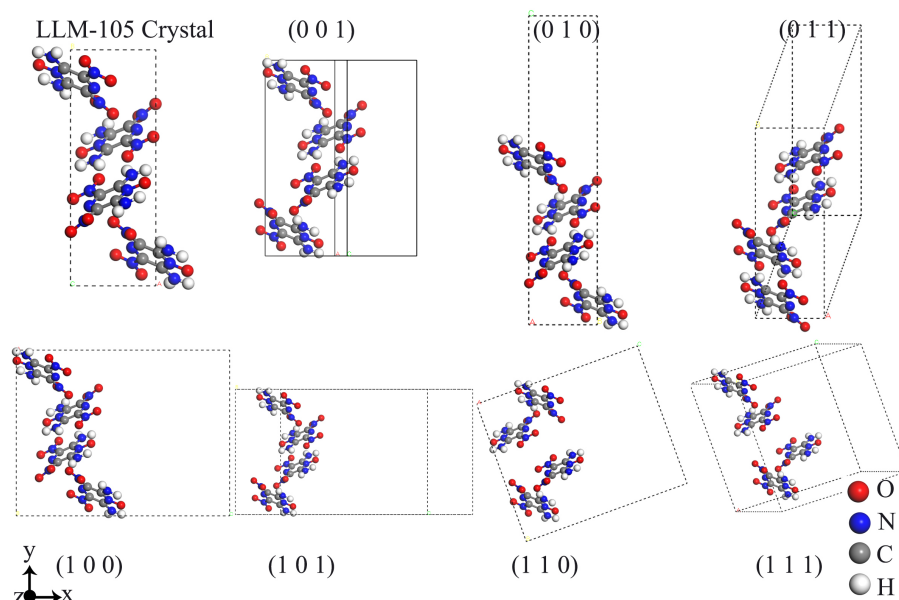


Figure 3. The crystal model and seven low-Miller-index planes of LLM-105.

2.1. Computational Details

All geometrical structures were calculated via CASTEP module of Materials Studio software (MS2017). The exchange-correlation function was treated by the Local Density Approximation (LDA) functional [11] and parameterized by CA-PZ [12] as it is reported that comparing to the generalized gradient approximation (GGA) [13] functions, LDA treatment could yield better results for the crystal structure studies of energetic systems [14,15]. The plane wave basis [16] set of pseudopotentials is used in the CASTEP model to calculate the properties of LLM-105 crystal and planes. The value of basis set correction [17] $dE_{\text{tot}}/d \log(E_{\text{cut}})$ can be used to indicate the convergence of the calculations with respect to the value of cut-off energy. According to the results of convergence tests in this study, the value of $dE_{\text{tot}}/d \log(E_{\text{cut}})$ for the 340 eV cut-off energy was smaller than 0.1 eV/atom, therefore, this value of E_{cutoff} is sufficient to achieve good convergence for the calculations. The convergence of k-points is achieved with a $4 \times 4 \times 1$ grid [18], as the equilibrium geometry parameters and the value of the total energy showed insignificant variations after increasing the number of k points from $4 \times 4 \times 1$ to $5 \times 5 \times 1$ or $6 \times 6 \times 1$. Therefore, it can be concluded that this value of k point was sufficient to calculate the correct energy values for the cases tested in this study. Periodic boundary conditions were used in the bulk and surface slab models. The Ultrasoft Vanderbilt Pseudopotentials (US-PP) with a plane basis set was used to describe the interaction between electrons and ions. In the following calculations, the slab model was used to study the surface properties of LLM-105 crystal and seven low-Miller-index planes.

The $1 \times 2 \times 2$ super cells of seven low-Miller-index planes of LLM-105 were modeled so as to avoid the interaction of large-size molecules with each other. There were 64 C, 64 H, 96 N and 80 O atoms existed in each plane for the seven low-Miller-index models. These models contained all the typical features of the L(011), L(001), L(010), L(100), L(101), L(110), and L(111). The surface sizes of the seven low-Miller-index planes of LLM-105 is presented in Table 3. The valence states considered in all the calculations were C- $2s^2 2p^2$, N- $2s^2 2p^3$,

H-1s¹ and O-2s²2p⁴. The Broyden–Fletcher–Goldfarb–Shanno (BFGS) method was utilized to optimize the LLM-105 crystal structures. The convergence criteria for plane properties calculation and geometric optimization of LLM-105 were set as following: (a) an energy tolerance of 5×10^{-6} eV/atom; (b) a self-consistent field tolerance of 5×10^{-7} eV/atom; (c) a maximum displacement tolerance of 5.0×10^{-4} Å; (d) a maximum force tolerance of 0.01 eV/Å. Tests on the stability of the structure and the relative energies with the increasing of the accuracy of the parameters were performed, which justified the selection of these parameters. All slab models were separated by a vacuum space with vacuum thickness of 20.0 Å to avoid the interactions between the images of the slab in the neighboring cells. The atoms in the bottom layer of the LLM-105 crystal surfaces were fixed while the upper atomic layer of the LLM-105 crystal surfaces were fully relaxed during the optimization process to reduce computational cost.

2.2. Surface properties

The surface energies of our slab models were calculated via equation (2),

$$E_{surf} = (E_{slab} - N \cdot E_{bulk}) / (2S) \quad (1)$$

where E_{bulk} is the reference energy for a LLM-105 unit in bulk phase and E_{slab} is the total energy of the supercell of a LLM-105 plane, S is the surface area of one side of the slab depending on the considered face and N is the number of LLM-105 units in the supercell. All atomic positions were able to relax during calculations.

There are two kinds of oxygen atoms existed in the L(101) (Figure 4) plane. A divalent oxygen atom and a monovalent oxygen atom (labeled as O2 and O3 in Figure 4). The bond length between the divalent oxygen atom and nitrogen atom (O2 and N5) is a little shorter than that between the monovalent oxygen atom and nitrogen atom (O3 and N5), and the bond length of O2-N5 is 1.217 Å, and the bond length of O3-N5 is 1.251 Å. The model of L(001) supercell is presented in Figure 4.

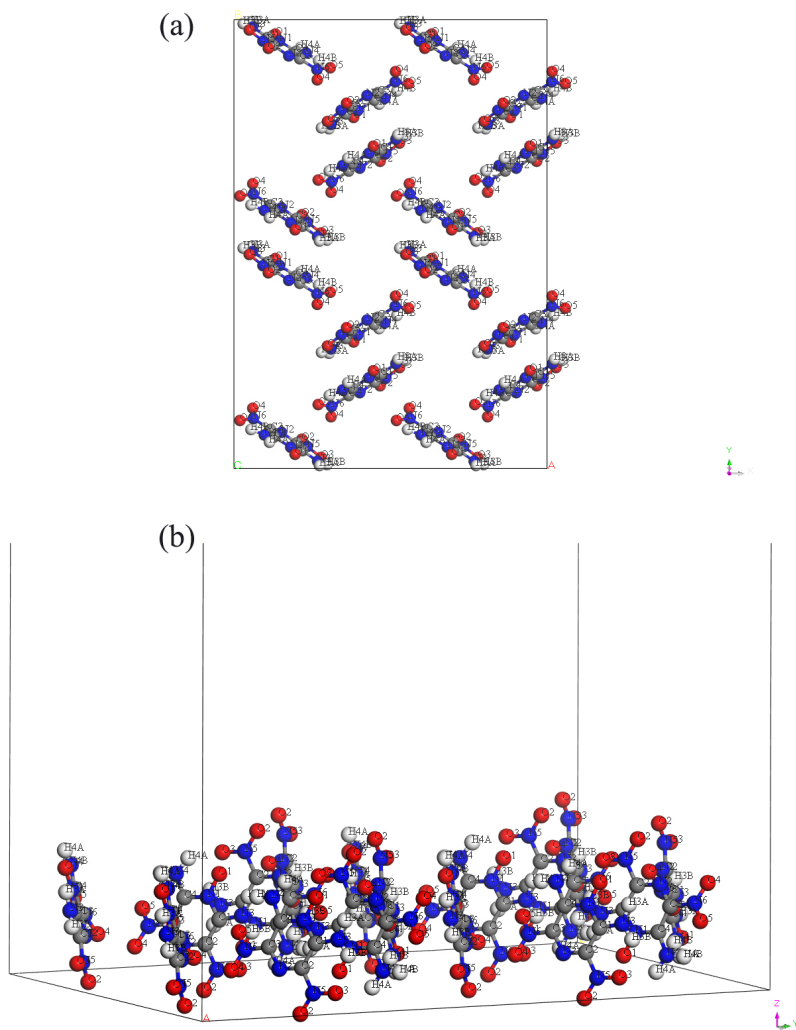


Figure 4. The 1×2×2 supercell model of L(101). (a) Top view, (b)Side view.

3. Results and Discussion

3.1. Bulk propoerties

To ensure the validity of the computational results, the calculated bulk lattice constants and surfaces energies were compared with data of other literatures. The lattice constants predicted in this paper are $a = 5.640 \text{ \AA}$, $b = 15.308 \text{ \AA}$ and $c = 8.156 \text{ \AA}$ for LLM-105, which are in good agreement with the experimental values ($a = 5.7430(11) \text{ \AA}$, $b = 15.825(3)$ and $c = 8.393(17) \text{ \AA}$)[9]. The detail lattice parameters of LLM-105 used in our computations were compared with those of other published literature and the comparison is presented in Table 1, demonstrating that the parameters of our LLM-105 were accurate and suitable for further calculations.

Table 1. Comparison of lattice parameters for LLM-105.

| | a(Å) | b(Å) | c(Å) | $\beta(^{\circ})$ |
|---------|-----------|-------------|-----------|-------------------|
| EXP[10] | 5.71-5.75 | 15.60-15.87 | 8.41-8.48 | 101.01-101.22 |
| PBE[19] | 5.64 | 15.96 | 8.46 | 100.93 |
| LDA[6] | 5.84 | 15.58 | 8.22 | 99.51 |
| PW91[6] | 6.01 | 18.28 | 8.71 | 100.75 |
| Ours | 5.64 | 15.31 | 8.16 | 100.78 |

¹ This is a table footnote.

Table 2. Structure Parameters for LLM-105.

| structural parameters | EXP[6] | LDA[6] | Ours |
|------------------------|--------|--------|-------|
| Bond Length (Å) | | | |
| B(C1-C2) | 1.407 | 1.411 | 1.429 |
| B(C2-N2) | 1.315 | 1.310 | 1.312 |
| B(N1-C1) | 1.368 | 1.381 | 1.381 |
| B(N2-C3) | 1.314 | 1.308 | 1.311 |
| B(C3-C4) | 1.406 | 1.427 | 1.423 |
| B(C4-N1) | 1.371 | 1.380 | 1.381 |
| Bond Angle (°) | | | |
| A(C1-C2-N2) | 124.3 | 123.6 | 122.9 |
| A(C2-N2-C3) | 118.1 | 119.7 | 119.6 |
| A(N1-C1-C2) | 115.1 | 115.5 | 115.8 |
| A(N2-C3-C4) | 123.6 | 123.0 | 123.7 |
| A(C3-C4-N1) | 115.8 | 115.5 | 115.4 |
| A(C4-N1-C1) | 122.9 | 122.6 | 122.5 |

3.2. Surface Energies

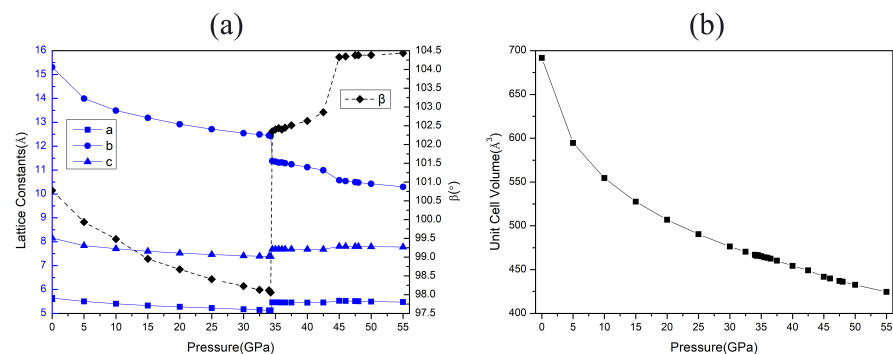
The results of surface Energy for each low-Miller-index plane is presented in Table 3, as we can see, L(101) and L(110) has lowest surface energy comparing to other plane. For example, the surface energy values of L(011), L(110) and L(101) is in the sequence of $L(011) > L(110) > L(101)$, which is verified in recent studies[20,21].

Table 3. Surface Energy of Seven low-Miller-index planes.

| Plane Name | E_{slab} (eV) | surface size(Å ²) | Energy(J/M ²) |
|------------|-----------------|-------------------------------|---------------------------|
| L(001) | -72483.7457 | 363.53 | 5.36 |
| L(010) | -36261.2058 | 189.28 | 4.33 |
| L(011) | -72501.6186 | 409.86 | 4.40 |
| L(100) | -72415.8043 | 531.28 | 4.69 |
| L(101) | -72711.6519 | 698.51 | 0.17 |
| L(110) | -72712.585 | 563.99 | 0.20 |
| L(111) | -72330.4431 | 723.70 | 4.39 |

3.3. LLM-105 crystal properties under high pressure

It is well known that the external pressure may result in changes of crystal phase transitions, molecular conformation and even changes of electronic structures. The lattice constants (a , b , c , β) of LLM-105 crystal at different pressures are presented in Figure 5(a). As we can see that, there is an obvious difference of how the values of a , b , c and β change at different pressures.

**Figure 5.** The lattice parameters at different pressure (a) Lattice constants (b) Unit Cell Volume.

The a-axis and c-axis decreases rapidly in the pressure range 0–5 GPa and then decreases slowly in the range 5–35 GPa. After that, it increases suddenly at a pressure of 35 GPa and then it increases rapidly in the range 42.5–45 GPa, and then it increases very slowly with the pressure increases. However, the b-axis decreases rapidly in the pressure range 0–10 GPa and then decreases slowly in the range 10–35 GPa. After that, it decreases suddenly at a pressure of 35 GPa and then it increases rapidly in the range 42.5–45 GPa, and then it decreases very slowly with the pressure increases.

The β value decreases rapidly in the pressure range 0–35 GPa and it increases suddenly at the pressure of 35 GPa and then it increases very slowly with the pressure increases. It should be noted that there is a rapid increase in the range 42.5–45 GPa. Besides, the unit cell volume of LLM-105 crystal at different pressure is presented in Figure 5(b). As we can see, the volume decreases with the pressure increases.

In the electron volts, the band gap normally means the distance between the bottom of the conduction band and the top of the valence band. The band gap of LLM-105 crystal at different pressures range 0–55 GPa are presented in Figure 6. Overall, the band gap value decreases with the external pressure increases, and there are two obvious sharp drops at 35 and 45 GPa that may be caused by structural transitions [2,6]. Besides, there is a slight increase of band gap in the pressure range 45–55 GPa, this increase may be caused by the shift of conduction bands to higher energy level. Similar band gap behavior was reported by other researchers [2,6] which verifies our results. It is assumed that with the external pressure increases, the overlap of different electronic bands increases, and then leads to the decrease of the inter-molecular space. However, when the external pressure keeps increasing after 45 GPa, there may be new twelve-membered ring forms and that may convert the molecule into a bigger conjugated system, which is more stable under pressure than previous structure.

It is reported that the impact sensitivity of energetic crystal (such as TATB [22], HMX [23], CL-20 [24], etc.) is related to many factors including band gap of that crystal. For these energetic crystals, smaller band gap means it is easier for electrons to jump from the valence bands to the conduction bands and that will increase the potential of that energetic material to decompose or even to explode. Which means, it can be inferred that when the external pressure increases, the impact sensitivity of LLM-105 will rise also.

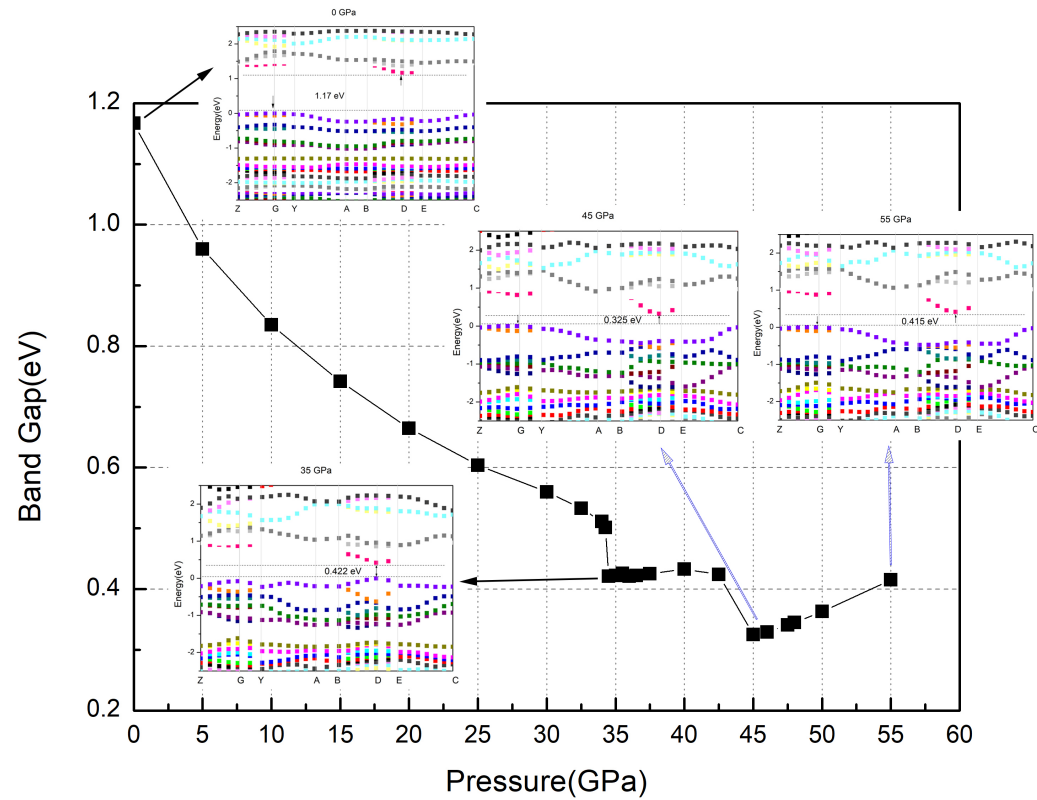


Figure 6. The band gap values of LLM-105 at different pressure .

In order to visualize the electronic density evolution at different pressures, the total electronic density map of LLM-105 crystal at the pressure 0 GPa and 45 GPa is presented in Figure 7 at an isovalue of 0.1 with the transparency of 10%. A slice parallel to a and b axis is added onto the crystal and transparency is set to 50%. As we can see, the crystal structure at 45 GPa is obviously smaller than that at 0 GPa. The volume of LLM-105 crystal at 0 GPa is 691.727 \AA^3 and that at 45 GPa is 441.765 \AA^3 .

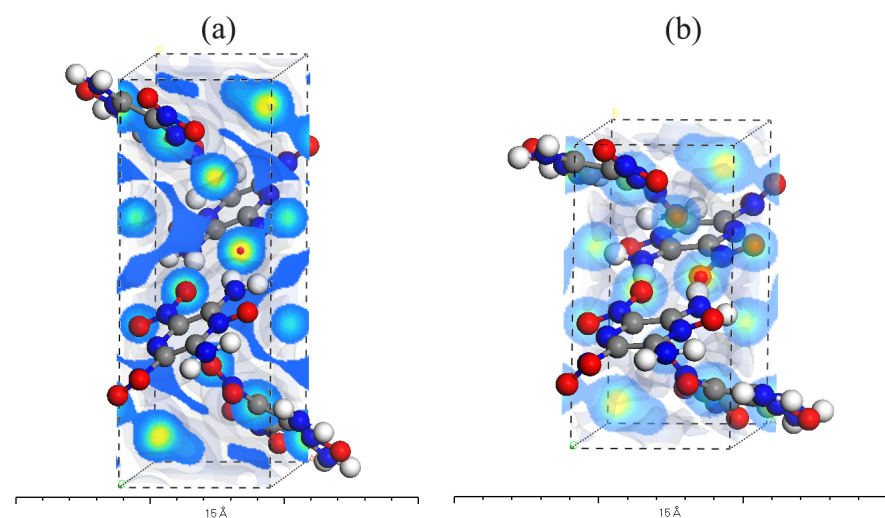


Figure 7. The total electronic density map of LLM-105 at 0 GPa and 45 GPa (a) 0 GPa (b) 45 GPa.

To determine the electronic states of the LLM-105 crystal under different pressures in the range 0-55 GPa, the total density of states (TDOS) and partial density of states (PDOS) at different pressures were calculated and the results were presented in Figure 8.

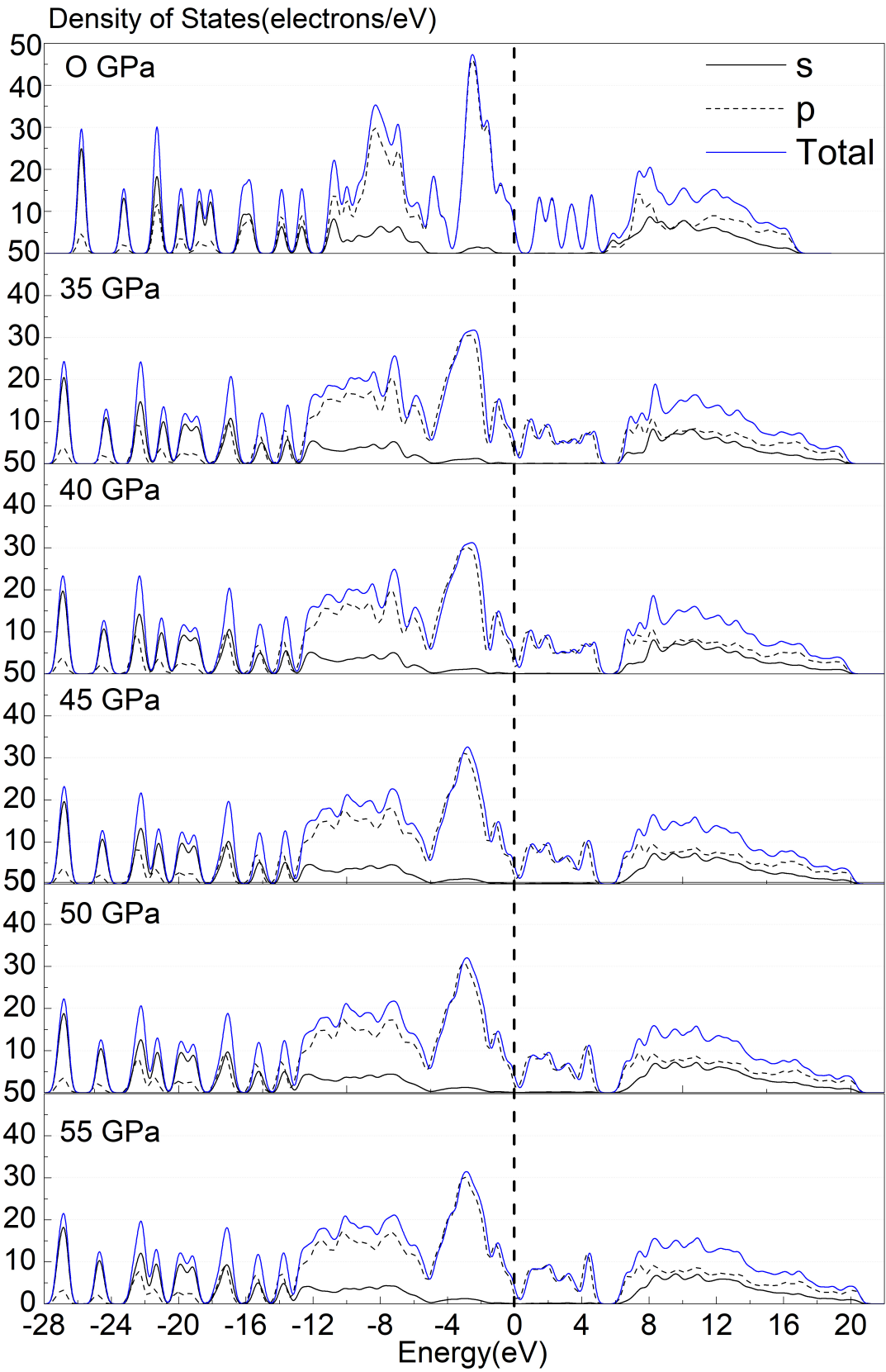


Figure 8. PDOS and TDOS of LLM-105 at 0, 35, 40, 45, 50, 55 GPa .

The main features of the Density of States at different pressures can be summarized as follows. Firstly, for the DOS at 0 GPa, the DOS curve is composed of several peaks, and when the pressure increases, the peaks in the valence bands seem to be more broader and dispersed, and the peak heights decrease, this phenomena may be caused by the enhanced intermolecular interactions when external pressure increases. Secondly, for the DOS peaks in the conduction and valence bands near the Fermi levels, the total states is mainly composed of p states, which means that p states dominates the chemical reactions of LLM-105. Thirdly, the behavior of the conduction bands is different between the range 0-45 GPa and the range 45-55 GPa, in the range 0-45 GPa, the conduction bands shows a shift to lower energies, however, in the range 45-55 GPa, the conduction bands shows a slight shift to higher energies, and this phenomena is in good agreement with the band gap result presented in Figure 6.

3.4. *L(101) properties under high pressure*

The band gap of L(101) at different pressures range 0-55 GPa are presented in Figure 9. Overall, the band gap value decreases with the external pressure increases, and there are two obvious sharp drops at range 5-10 GPa and 40-50 GPa. Besides, there is a slight increase of band gap in the pressure range 10-20 GPa, this increase may be caused by the shift of conduction bands to higher energy level.

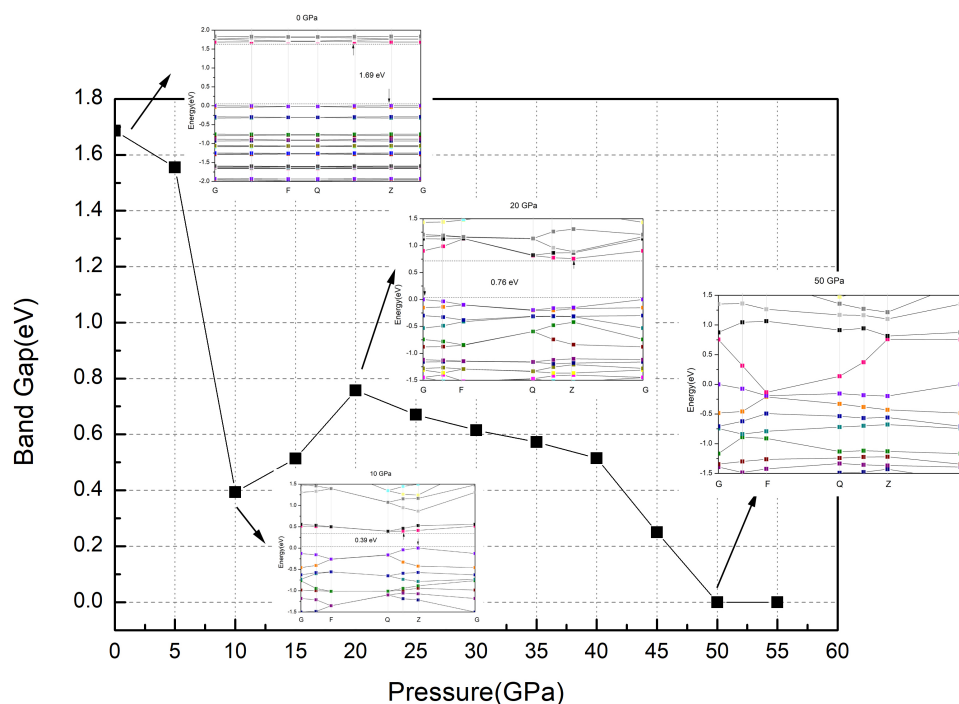


Figure 9. The band gap values of L(101) at different pressure.

the total electronic density map of L(101) at the pressure 10 GPa and 55 GPa is presented in Figure 10 at an isovalue of 0.1 with the transparency of 10%. A slice parallel to a and b axis is added onto the crystal and transparency is set to 50%. As we can see, the crystal structure at 55 GPa is obviously smaller than that at 10 GPa. The volume of L(101) at 10 GPa is 570.014 Å³ and that at 55 GPa is 412.953 Å³.

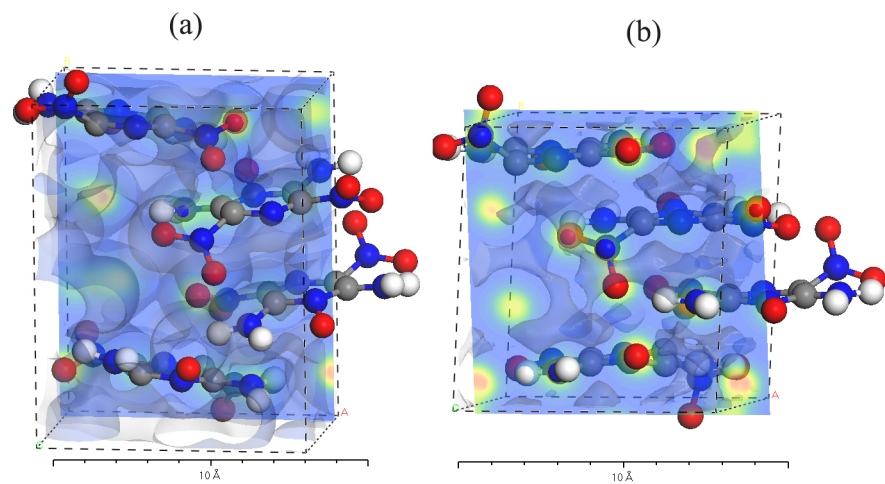


Figure 10. The total electronic density map of LLM-105 at 10 GPa and 55 GPa (a) 10GPa (b) 55GPa.

To determine the electronic states of the L(101) under different pressures in the range 0-55GPa, the total density of states(TDOS) and partial density of states(PDOS) at different pressures were calculated and the results were presented in Figure 11.

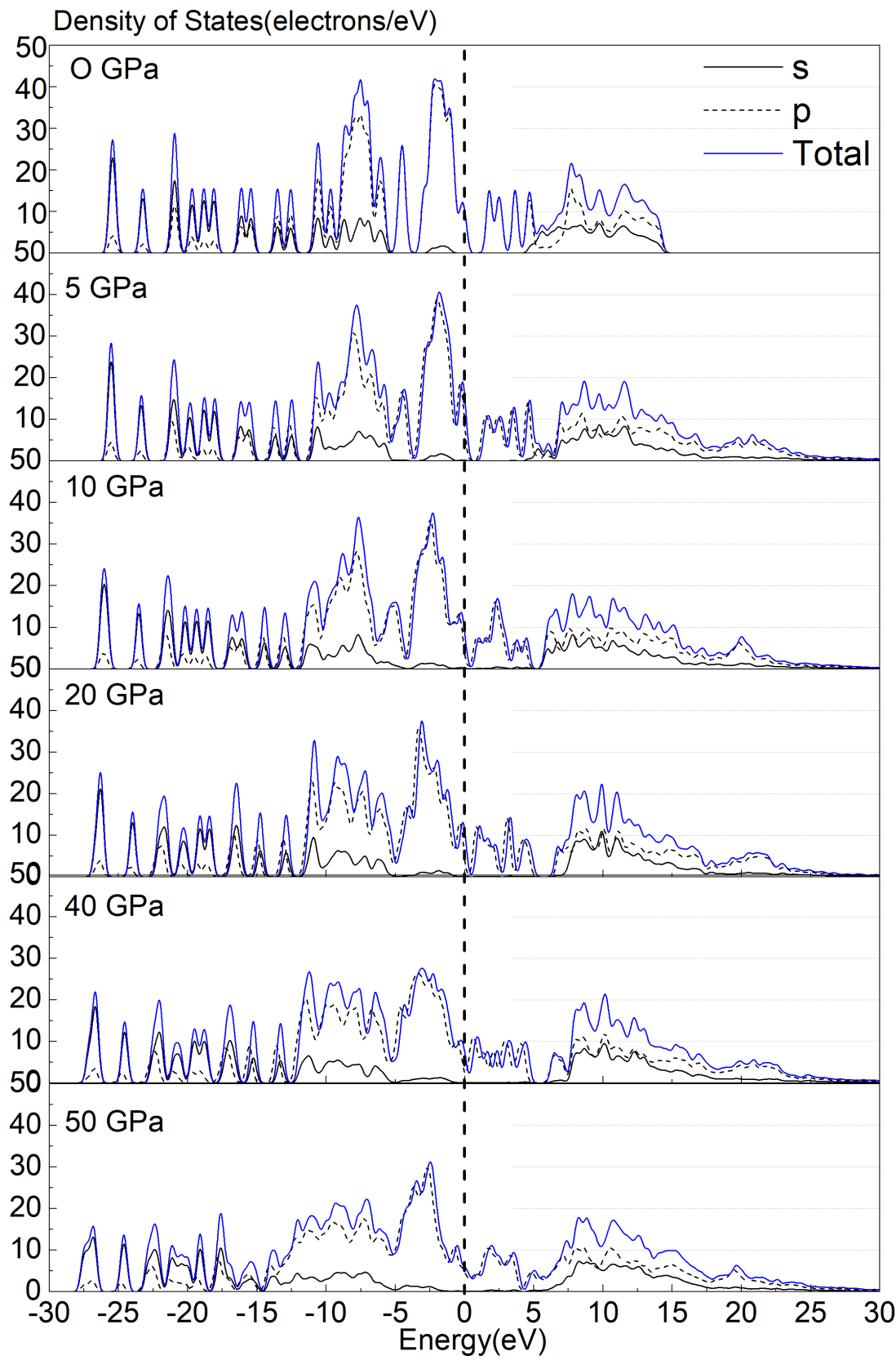


Figure 11. PDOS and TDOS of L(101) at 0, 35, 40, 45, 50, 55 GPa .

As we can see in Figure 11, for the DOS near the pressure of 0 GPa, the DOS curve is composed of several peaks and it is mainly composed of p states. When the pressure increases, it is obvious that the peaks in the valence bands become more broader and dispersed, and the peak heights decrease obviously when the pressure is bigger than 20 GPa, this phenomena may be caused by the enhanced intermolecular interactions when external pressure increases. What's more, for the DOS peaks in the conduction and valence bands near the Fermi levels, the total states is mainly composed of p states. And finally, the behavior of the conduction bands is different in three pressure ranges: the range 0-10 GPa, the range 10-20 GPa and the range 20-55 GPa, in the range 0-10 GPa, the conduction bands shows a shift to lower energies, however, in the range 10-20 GPa, the conduction bands shows a slight shift to higher energies. In the meantime, it can be observed that when the external pressure is bigger than 50 GPa, it seems that the band gap value of L(101) becomes zero, which means L(101) will become highly sensitive at the pressure bigger than 50 GPa.

4. Conclusions

The electronic structural evolution of LLM-105 crystal and the (101) plane of LLM-105 crystal under different pressures is investigated by the density functional theory (DFT) calculations and the surface properties of seven low-Miller-index planes of LLM-105 crystal were investigated in this study. The results confirmed that L(101) has the lowest surface energy compared with other low-Miller-index planes and the LLM-105 crystal presents an indirect band structure with a band gap of about 1.2 eV at 0 GPa pressure. As the plane with lowest energy, L(101) demonstrated good stability under high pressure and a shift in DOS can be observed from the theoretical results, besides, the electronic structures of LLM-105 crystal and the (101) plane changed with the increase of external pressure and the evolution process of (101) plane is different from that of LLM-105 crystal structure.

Author Contributions: Conceptualization, Gang He and Wenkun Zhu; methodology, Gang He, Zhiqiang Qiao; validation, Gang He, Zhengguo Chen; formal analysis, Zhengguo Chen; writing—original draft preparation, Gang He; writing—review and editing, Jun Wen, Zhengguo Chen; All authors have read and agreed to the published version of the manuscript. 'First-Principles study of the electronic structure of LLM-105 crystal and (101) plane under high Pressure'

Funding: This work was supported by NSFC (No. 21976147, 21906154, and 21902130), Sichuan Science and Technology Program (No. 2020YFG0467 and 2019ZDZX0013, NO.2020YFS0454, NO.2020YFS0318, NO.2020YFG0430), the Project of State Key Laboratory of Environment-friendly Energy Materials in SWUST (No. 20fksy19 and 21zd3366), NHC Key Laboratory of Nuclear Technology Medical Transformation (MIANYANG CENTRAL HOSPITAL) (Grant No.2021HYX031), and Research Fund of SWUST for PhD (No. 18zx7149 and 19zx7129).

Data Availability Statement: Not applicable.

Conflicts of Interest: The authors declare no conflict of interest. The funders had no role in the design of the study; in the collection, analyses, or interpretation of data; in the writing of the manuscript, or in the decision to publish the results.

Abbreviations

The following abbreviations are used in this manuscript:

| | |
|---------|--|
| LLM-105 | 2,6-diamino-3,5-dinitropyrazine-1-oxide |
| HMX | octahydro-1,3,5,7-tetranitro-1,3,5,7-tetrazocine |
| TATB | 1, 3, 5-triamino-2, 4, 6-trinitrobenzene |
| CASTEP | Cambridge Sequential Total Energy Package |
| DFT | Density Functional Theory |
| LDA | Local Density Approximation |
| GGA | Generalized Gradient Approximation |
| BFGS | Broyden–Fletcher–Goldfarb–Shanno |

References

1. Pasquinet, E.; Pin, N.; Forzy, A.; Palmas, P.; Rideau, J.; Beaucamp, A.; Lalière, E.; Perdrigeat, M.L.; Quéré, S.; Barthet, C.a. DAPmmLM5: Improving the Particle Morphology and Thermal Stability. *Propellants Explosives Pyrotechnics* **2019**.
2. Xu, Z.; Chen, Q.; Li, X.; Wang, J.; Zhang, Z. Electronic Structure of LLM-105 Crystal under High Pressure and Low Temperature. *The Journal of Physical Chemistry C* **2020**, XXXX.
3. Xu, W.; An, C.; Wang, J.; Dong, J.; Geng, X. Preparation and Properties of An Insensitive Booster Explosive Based on LLM-105. *Propellants Explosives Pyrotechnics* **2013**, 38, 136–141.
4. Pagoria, P.; Zhang, M.X.; Zuckerman, N.; Lee, G.; Mitchell, A.; DeHope, A.; Gash, A.; Coon, C.; Gallagher, P. Synthetic Studies of 2,6-Diamino-3,5-Dinitropyrazine-1-Oxide (LLM-105) from Discovery to Multi-Kilogram Scale. *Propellants, Explosives, Pyrotechnics* **2018**, 43, 15–27.
5. Gilardi, R.D.; Butcher, R.J. 2,6-Diamino-3,5-dinitro-1,4-pyrazine 1-oxide. *Acta Crystallographica Section E Structure Reports Online* **2001**.
6. Wu, Q.; Yang, C.; Yong, P.; Fang, X.; Liu, ..., Z. First-principles study of the structural transformation, electronic structure, and optical properties of crystalline 2,6-diamino-3,5-dinitropyrazine-1-oxide under high pressure. *Journal of Molecular Modeling* **2013**, 19, 5159–5170.
7. Stavrou, E.; Riad Manaa, M.; Zaug, J.M.; Kuo, I.F.W.; Pagoria, P.F.; Kalkan, B.; Crowhurst, J.C.; Armstrong, M.R. The high pressure structure and equation of state of 2,6-diamino-3,5-dinitropyrazine-1-oxide (LLM-105) up to 20 GPa: X-ray diffraction measurements and first principles molecular dynamics simulations. *Journal of Chemical Physics* **2015**, 143, 1209.
8. Zuckerman, N.B.; Shusteff, M.; Pagoria, P.F.; Gash, A.E. Microreactor Flow Synthesis of the Secondary High Explosive 2,6-Diamino-3,5-dinitropyrazine-1-oxide (LLM-105). *Journal of Flow Chemistry* **2015**, 5, 178–182.
9. Liu, J.J.; Liu, Z.L.; Cheng, J. Synthesis, Crystal Structure and Catalytic Properties of Two Energetic Complexes Containing 2,6-Diamino-3,5-dinitropyrazine-1-oxide. *Chinese Journal of Inorganic Chemistry* **2014**, 30, 696–704.
10. Wang, X.; Zeng, Q.; Li, J.; Yang, M. First-Principles-Based Force Field for 2,6-Diamino-3,5-dinitropyrazine-1-oxide (LLM-105). *ACS Omega* **2019**, XXXX.
11. CePerley, D.M.; Alder, B.J. Ground State of the Electron Gas by a Stochastic Method. *Physical Review Letters* **1980**, 45, 566–569.
12. Perdew, J.P.; Zunger, A. Self-Interaction Correction to Density-Functional Approximations for Many-Body Systems. *Physical review. B, Condensed matter* **1981**, 23, 5048–5079.
13. Perdew, J.P.; Burke, K.; Ernzerhof, M. Phys. Rev. Lett. 77, 3865 (1996): Generalized Gradient Approximation Made Simple **1996**.
14. Manaa, M.R.; Kuo, I.; Fried, L.E. First-principles high-pressure unreacted equation of state and heat of formation of crystal 2,6-diamino-3,5-dinitropyrazine-1-oxide (LLM-105). *The Journal of Chemical Physics* **2014**, 141, 064702.
15. Zhu, W.; Zhang, X.; Tao, W.; Xiao, H. DFT studies of pressure effects on structural and vibrational properties of crystalline octahydro-1,3,5,7-tetranitro-1,3,5,7-tetrazocine. *Theoretical Chemistry Accounts* **2009**, 124, 179–186.
16. Clark, S.J.; Segall, M.; Pickard, C.J.; Hasnani, P.J.; Probert, M. First principles methods using CASTEP. *Zeitschrift für Kristallographie - Crystalline Materials* **2005**, 220.
17. Francis, G.P.; Payne, M.C. Finite basis set corrections to total energy pseudopotential calculations. *Journal of Physics Condensed Matter* **1999**, 2, 4395.
18. Monkhorst, H.J.; Pack, J.D. Special points for Brillouin-zone integrations. *Physical review. B, Condensed matter* **1976**, 13, 5188–5192.
19. Bergh.; Magnus.; Coleman.; Carl. A Validation Study of the General Amber Force Field Applied to Energetic Molecular Crystals. *Journal of Energetic Materials* **2016**.
20. Ron, L.; Qiang, G.; Qian, Y.; Nian-shou, C.; Chang-gen, F. Molecular Dynamics Simulation on Crystal Morphology of LLM-105. *Chinese Journal of Explosives & Propellants* **2018**, 41, 7.
21. adn AN Chongwei, L.B.; Shuai, X. Molecular Dynamics Simulation on Crystallization Morphology of LLM-105 in Different solvents. *Journal of Ordnance Equipment Engineering* **2019**, 40, 6.
22. Yan-Qun, W.; Jun, W.; Hui-Sheng, H.; Zhi-Qiang, Q.; Rui, L.I.; Jin-Peng, S.; Guang-Cheng, Y. Structure and Formation Mechanism of Impurity in Nano-TATB. *Hanneng Cailiao/Chinese Journal of Energetic Materials* **2016**, 24, 604–608.
23. First-Principles Study of the Four Polymorphs of Crystalline Octahydro-1,3,5,7-tetranitro-1,3,5,7-tetrazocine. *The Journal of Physical Chemistry B* **2007**, 111, 12715–12722.
24. Zhu, W.H.; Xiao, H.M.; Xu, X.J. DFT studies on the four polymorphs of crystalline CL-20 and the influences of hydrostatic pressure on epsilon-CL-20 crystal. *The Journal of Physical Chemistry B* **2007**, 111, 2090–7.